



Original Article

Investigation of the manufacturing processes type and post processing effects on the mechanical and microstructural properties of eco-friendly brass alloys

Nima ZOGHIPOUR^{1,2}, Yusuf KAYNAK²

¹Torun Copper Alloy Metal Ind. & Ltd. Inc., Kocaeli, Türkiye

²Department of Mechanical Engineering, Marmara University, İstanbul, Türkiye

ARTICLE INFO

Article history

Received: 01 November 2022

Revised: 29 April 2023

Accepted: 17 May 2023

Key words:

Annealing, brass, forging, mechanical and microstructural properties.

ABSTRACT

Brass materials are categorized in the copper alloys sub-groups with prevailing Zinc element. These materials are utilized from drinking water systems to automotive in a wide range of industrial applications due to superior properties such as strength, formability and corrosion resistance. This study aims to characterize and analyze smart and popular conducted manufacturing processes influences on the mechanical and microstructural properties of eco-friendly brass alloy. In this regard, microstructural, hardness, tensile and impact charpy tests have been carried out on extruded, extruded+annealing, forged and forged+annealing eco-brass CuZn40Pb2, CuZn38AS, CuZn21Si3P specimens. The experimental results have demonstrated that the manufacturing process type extremely influences the materials mechanical and microstructural properties.

Cite this article as: Zoghipour, N., & Kaynak, Y. (2023). Investigation of the manufacturing processes type and post processing effects on the mechanical and microstructural properties of eco-friendly brass alloys. *J Adv Manuf Eng*, 4(1), 77–87.

INTRODUCTION

Being in the main Cu-Zn alloy category, brass material is extensively used in industry due to its outstanding properties, including exceptional corrosion resistance, electric and thermal conductivity, good plasticity formability, recyclability and machinability [1]. Lead coalescence negatively affects machinability by increasing mean particle size and decreasing Pb particle density [2]. While excess lead or an irregular lead distribution may induce surface cracking during hot working owing to hot shortness, a fine and uniform lead distribution expedites machining processes by improving chip fracturing and reducing tool wear [3]. Because friction between the billet and container raises the extrusion's temperature, hot shortness is the result of over-

heating. Leaded brass alloys' phase structure is controlled by a variety of mechanisms. The α/β interphase boundaries are possible distribution points for lead since they are places with significant interfacial energy [4]. Consideration has been given to material designs that will adhere to applicable regulations such as Restriction of Hazardous Substances (RoHS) and Waste Electrical and Electronic Equipment (WEEE) [5–9]. Since a large amount of the application of brass is in drinking water and pumping systems, from the basis of lead's potentially harmful impacts on both humans and the environment, its usage must be reduced [10, 11].

Leaded α - β brass (CW614N-Cu58Zn39Pb3) rods have been examined using light and scanning electron microscopy by Pantazopoulos et al. [2] to determine their main microstructural properties. Regarding the resulting ma-

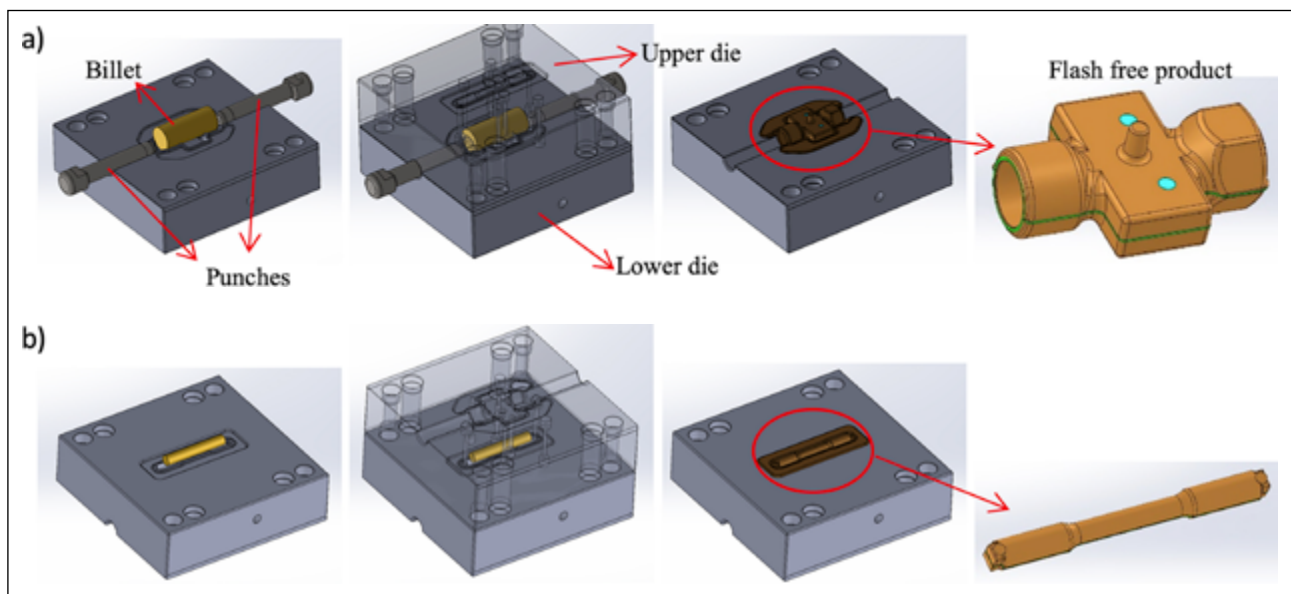
*Corresponding author.

*E-mail address: nima.zoghipour@gmail.com



Table 1. Chemical composition of the studied brass alloys [19]

Composition	Cu	Zn	Pb	Sn	Fe	Ni	Al	As	Mn	P	Si
CuZn40Pb2											
%Min.	57.0	Rem.	1.6	–	–	–	–	–	–	–	–
%Max.	59.0	Rem.	2.5	0.3	0.3	0.3	0.05	–	–	–	–
CuZn38As											
%Min.	61.5	Rem.	–	–	–	–	–	0.02	–	–	–
%Max.	63.5	Rem.	0.2	0.1	0.1	0.3	0.05	0.15	–	–	–
CuZn21Si3P											
%Min.	75.0	Rem.	–	–	–	–	–	–	–	0.02	2.7
%Max.	77.0	Rem.	0.09	0.3	0.3	0.2	0.05	–	0.05	0.10	3.5

**Figure 1.** Hot forging procedure of the designed test specimens; (a) case study product, (b) tensile test.

chability performance, critical factors like particle population density and particular interphase boundary lengths are examined. The impact of extrusion parameters on the phase structure of CuZn40Pb2 was investigated by Holler et al. [12]. They demonstrated that while grain size fell with reducing billet temperature and increasing extrusion ratio, the proportion of β -phase was lowered with increasing billet temperature and increasing extrusion ratio. The extrusion speed has a less impact on grain size and β -phase fraction. Stlnacke et al. [13] investigated three distinct novel low-lead and lead-free brass alloys under various annealing conditions, and the resultant microstructures are mapped in relation to their dezincification ability. Based on their research, it was found that alloys with higher aluminum and iron content only had the most severe loss of corrosion resistance. These alloys showed considerable precipitation of twins, lead, and intermetallic aluminum arsenide particles on grain boundaries, as well as the development of the β -phase along grain boundaries. In order to increase the machinability of three lead-free extruded and drawn brasses, namely CuZn42 (CW510L), CuZn38As (CW511L), and CuZn36 (C27450), Toulfatzis et al. [14] applied heat treat-

ment based on the theory of microstructural alteration. Chip morphology, power consumption, cutting force, and surface roughness were the machinability characteristics that were studied. In another work, Toulfatzis et al. [15] examined the mechanical properties of three lead-free brass alloys (CW510L, CW511L, and C27450) under static and dynamic stress in contrast to a traditional leaded brass alloy (CW614N). Two industrial copper alloys, CuZn39Pb3 and CuZn36Pb2As, were examined in connection to their microstructure for their primary fracture modes and mechanical properties by Pantazopoulos et al. [16]. They employed analytical methods in this inquiry optical metallography, macro- and micro-fractography, as well as static and dynamic mechanical testing. The leakage locations around the brazing position were the main topic of study for Chunlei et al. [17]. As the primary analytical techniques for the current failure investigation, visual examination, stereomicroscopy, and scanning electron microscopy combined with an energy dispersive spectrometer (SEM/EDS) were employed. The analysis's findings suggested that the failure of lead-free brass valve bodies was likely caused by the combined impact of high brazing residual stresses and

Table 2. Technical specifications of the extruded brass alloys

Brass alloy	Elasticity module (GPa)	Density (g/cm ³)	Electrical conductivity (MS/m)	Thermal conductivity (W/(m.K))	Coe. of thermal expansion (10 ⁻⁶ /K)	Melting point (°C)	Hot forming (°C)	Soft annealing (°C)	Soft annealing duration (h)	Stress relieving (°C)	Stress relieving duration (h)
CuZn40Pb2	96	8.43	14.9	113	21.1	880–895	650–800	450–600	1–3	200–300	1–3
CuZn38As	100	8.41	14.7	114	21.7	850–900	600–800	450–550	1–3	200–250	1–3
CuZn21Si3P	100	8.25	4.5	35	–	680–750	530–650	450–550	1–3	200–300	1–3

Table 3. The phasic percentages of the studied brass alloys

Brass type	α%	β%	κ% + γ%
CuZn40Pb2			
Extruded	54	46	–
Extruded & annealed	56	44	–
Forged	49	61	–
Forged & annealed	39	51	–
CuZn38As			
Extruded	94	6	–
Extruded & annealed	99	1	–
Forged	83	17	–
Forged & annealed	96	4	–
CuZn21Si3P			
Extruded	84	–	16
Extruded & annealed	89	–	11
Forged	81	–	19
Forged & annealed	84	–	16

bismuth boundary segregation. By using a cylindrical external turning method with polycrystalline diamond inserts, Amaral et al. [18] concentrated on the machinability characterization of three distinct brass alloys (lead, medium-lead, and minimally lead). Three different cut depths, three feed rates, and four cutting speeds were covered in parametric research. Analysis and comparison of cutting forces, chip shape, and surface roughness among alloys were done.

Considering the available studies conducted on this topic, it is seen that there are only a few investigations which have been concentrated on these types of brass alloys. However, there are no available carried out studies on the comparison of the effects of manufacturing type on the mechanical and microstructural properties of eco-friendly brass alloys especially CW724R. The purpose of this study is to describe and examine how innovative and widely used manufacturing techniques affect the mechanical and metallurgical characteristics of an environmentally friendly brass alloy. In this respect, tests on extruded, extruded+annealed, forged, and forged+annealed eco-brass CuZn40Pb2, CuZn38AS, and CuZn21Si3P specimens were performed on their microstructural, hardness, tensile, and impact properties.

Experimental Methodology

Lead CuZn40Pb2, low-lead CuZn38As, and lead-free CuZn21Si3P with a diameter 35 mm extruded (as re-

ceived) bars were selected as three brass alloy types in this study. The chemical composition and technical specifications of the mentioned materials are given in Table 1 and 2. Some of the rods were cut into the billets of Ø35 mm and 86 mm in length, and then forged at 730±10 °C with a rate of 11 stroke/min under a 165 tons of press load in a Hydromec 550 eccentric press machine as displayed in Figure 1a. Afterwards, annealing process were applied on them at 550 °C for 150 minutes. Furthermore, according to ASTM E8/E8M – 09 standards dimensions, tensile test specimens were also hot forging at 730±10 °C with 70 tons of press with a rate of 9 stroke/min. with the dimensions of 20 and 120 mm in diameter and length and then subjected to annealing as demonstrated in Figure 1b. Keyence digital optical microscope and SEM (Scanning electron microscopy) were used to examine the microstructural analyses of the specimens. The specimens were subjected to tensile testing at a strain rate of 2 mm/min. MHVD 1000 IS hardness tester equipment was used to conduct micro-hardness tests on the examined specimens under 100 g applied load for 10 seconds in accordance with ASTM E 384 criteria. The average value of five measurements is presented. The impact Charpy experiments were conducted using V-notched specimens in accordance with ASTM E23, and the average of two measurements of the notch impact energy are provided in this study.

RESULTS AND DISCUSSIONS

Microstructure Analyses

Figure 2 and 3 demonstrated the microstructural and phases of the extruded, extruded-annealed, forged and forged-annealed of CuZn40Pb2, CuZn38As and CuZn-21Si3P brasses. It is seen that the leaded (CuZn40Pb2) and low-lead brasses are formed of α and β phases from the microstructure inspection analyses while α , κ and γ phases are the main forming microstructure of lead-free brass (CuZn-21Si3P). The existence of Pb particles is also obvious as black spots in CuZn40Pb2 microstructure. It is well known that the lattice structure of α is FCC (Face centered cubic), the β , γ and Si-rich κ phases are BCC (Body centered cubic), and hexagonal, respectively.

Table 3 illustrates the phasic percentages of the mentioned brasses for extruded, extruded-annealed, forged and forged-annealed specimens. An increase has been obtained in % β by forging in all types of CuZn40Pb2 and CuZn38As. However, a reverse relation is accomplished by annealing on the mentioned alloys. An improvement of the machinability has been discussed with the positive commitment of β by several researchers [20]. Furthermore, annealing leads to a less hard surface and tool wear. The amount of the γ is very low as compared to α and κ . Therefore, by measuring the % κ in the microstructure, we can conclude to that the % α has increased with annealing whereas it has been decreased by forging.

Tensile Tests

The stress-strain graphical results of the tensile tests are demonstrated in Figure 4. The forged specimens displayed a semi-brittle behavior under strain with an unexpected rapid rupture. The lowest yield point for annealed CuZn38As bar was determined to be 110 MPa. However, 387 MPa was found to be the maximum value tested for forged CuZn-21Si3P. The obtained results for extruded specimens are in agreement with the obtainments in [20]. Additionally, the yield stress of the extruded bar was reduced by annealing by 15%, 19%, and 2% for CuZn40Pb2, CuZn38As, and CuZn-21Si3P, respectively, whereas these percentages were 16%, 41%, and 22% for the same forged materials. It is important to note that, for both extruded and forged brass alloys, annealing has resulted in a decrease in durability and an earlier onset of permanent plastic deformation zone due to a decline in the dislocations within the crystal structures. However, forging raised the yield stress by 58%, 52%, and 77% for CuZn40Pb2, CuZn38As, and CuZn21Si3P, respectively as shown in Figure 5. This outcome serves as an example of how working metal twice under tension compacts it and creates a grain structure that is dense and refined thanks to the application of two high pressures during rod extrusion and forging [21, 22]. Additionally, the calculation of the elastic modulus for the test specimens, which is also included in Table 4, validates the outcomes for the yield stress levels and their variation as a result of the annealing and forging processes. Figure 6 displays the specimens' ruptured pictures following the tensile test. As can be observed, every material has undergone a 45° fracture or rupture, which is a hint to a ductile fracture. The increase

in the progressively work in CuZn40Pb2 and CuZn38As in light of the increased number of slip frameworks and dislocation lattice friction stresses when compared with the phase, which is FCC, is thus anticipated to lead to a noticeable increase in the brittleness but improved durability. In addition, it is expected that CuZn21Si3P would exhibit brittleness because of the easier mobility of dislocations in HCP (Hexagonal Close-Packed) due to 3 slip frameworks when compared with FCC and BCC [23].

Hardness

The average value of five measurements for hardness tests is reported in Table 5. Extruded and annealed CuZn38As was found to have the lowest hardness, which was 88.8 HV. The greatest value, however, was determined to be 138.9 HV for the forged CuZn21Si3P. As it is seen from Figure 7, the lowering of the hardness attribute for the test materials is clearly caused by annealing when findings are seen in a wide context, as was done in this study. In the meantime, a rise in the hardness value is attained as a result of the movement of the dislocations and grain refinements in the alloy structures extracted by forging process. This hardness can be explained by Hall-Petch equation as given in below:

$$\sigma_y = \sigma_0 + K\sqrt{d} \quad (1)$$

Where σ_y , σ_0 , K and d stand for the yield stress, materials constant for the starting stress for dislocation movement, the strengthening coefficient, and the average grain diameter, respectively [24]. And using the Hal-Petch equation, it can be deduced that smaller grain sizes improve micro hardness because they impede the mobility of dislocations in the crystalline microstructure.

Impact Charpy testing is a technique used to estimate the energy needed for various materials to fracture under dynamic stresses. In other words, the outcome of this test exposes the fracture energy as a mechanical property [23]. The kind of notch, the material's yield stress, alloying elements, crystal structures, temperature, cooling, annealing, and forming conditions/procedures all have a significant impact on the microstructural phase, grain size type, and fracture behavior of the material. Therefore, it is clear that the fracture characteristic is closely related to the materials' chip breakability and machinability [15, 23]. The average of two measurements of the notch impact energy is reported in Table 6. The results show that annealing enhanced the toughness value for CuZn40Pb2, CuZn21Si3P, and CuZn38As by 11.34%, 88.02%, and 14.24%, respectively. This trend is in discrepancy for CuZn38As in [15]. However, they had different annealing parameters as compared to the deployed ones in this study. In the case of forged specimens, annealing resulted in increases in the fracture energy values of CuZn40Pb2, CuZn21Si3P, and CuZn38As of 4.03%, 20.70%, and 2.64%, respectively. According to the findings of the Charpy impact experiment, annealing enhances the material's capacity to absorb energy. In α + β brasses, annealing results in the increase of the β phase percentage as demonstrated in microstructural studies section of this chapter. In the following, the hardness value drops.

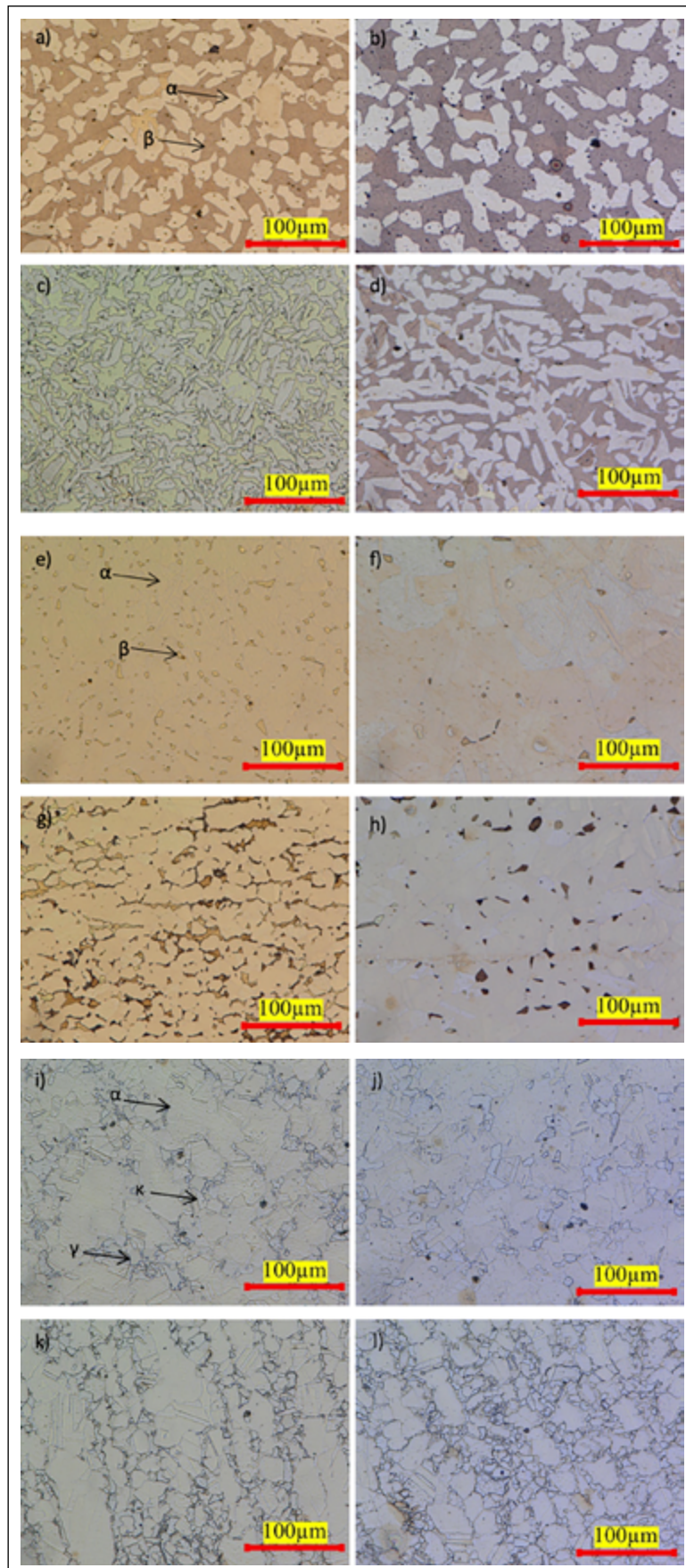


Figure 2. Optical images of the microstructure of, CuZn40Pb₂; (a) extruded, (b) extruded-annealed, (c) forged, (d) forged-annealed, CuZn38As; (e) extruded, (f) extruded-annealed, (g) forged, (h) forged-annealed, CuZn21Si3P; (i) extruded, (j) extruded-annealed, (k) forged, (l) forged-annealed.

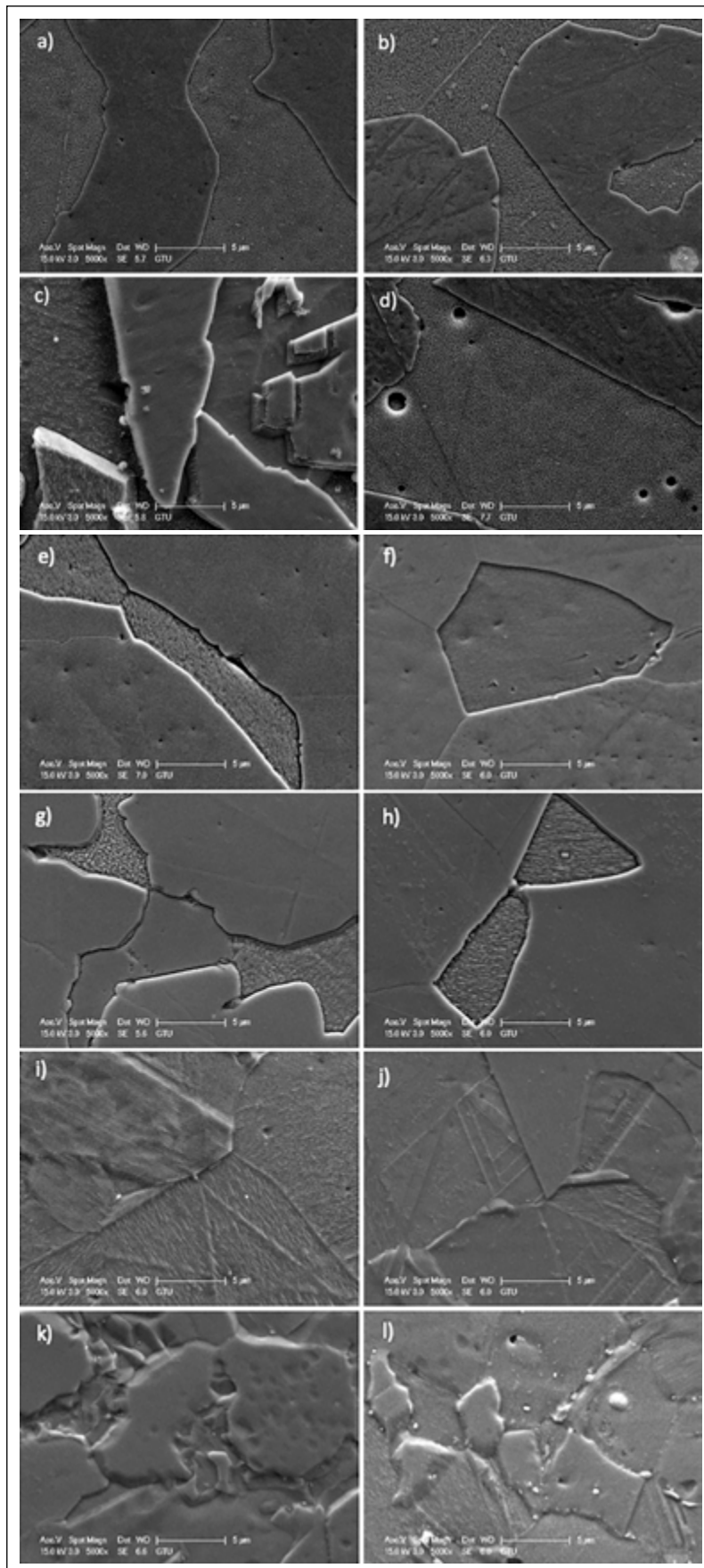


Figure 3. SEM images of the microstructure of, CuZn40Pb₂; (a) extruded, (b) extruded-annealed, (c) forged, (d) forged-annealed, CuZn38As; (e) extruded, (f) extruded-annealed, (g) forged, (h) forged-annealed, CuZn21Si3P; (i) extruded, (j) extruded-annealed, (k) forged, (l) forged-annealed.

Table 4. The experimental mechanical properties of the studied brass alloys

Brass alloy type	Yield stress, (MPa)	Ultimate tensile stress, (MPa)	Elastic modulus, (GPa)
CuZn40Pb2 Extruded	153	442.4	84.8
CuZn40Pb2 Extruded-annealed	130	420	85.48
CuZn40Pb2 Forged	243	399.2	77.35
CuZn40Pb2 Forged-annealed	203	428.9	74.48
CuZn38As Extruded	136	366.6	82.81
CuZn38As Extruded-annealed	110	351.2	87.07
CuZn38As Forged	208	393.9	80.46
CuZn38As Forged-annealed	141	356.9	79.33
CuZn21Si3P Extruded	218	522.7	78.76
CuZn21Si3P Extruded-annealed	213	547.3	78.40
CuZn21Si3P Forged	387	550.9	75.71
CuZn21Si3P Forged-annealed	299	563.9	77.01

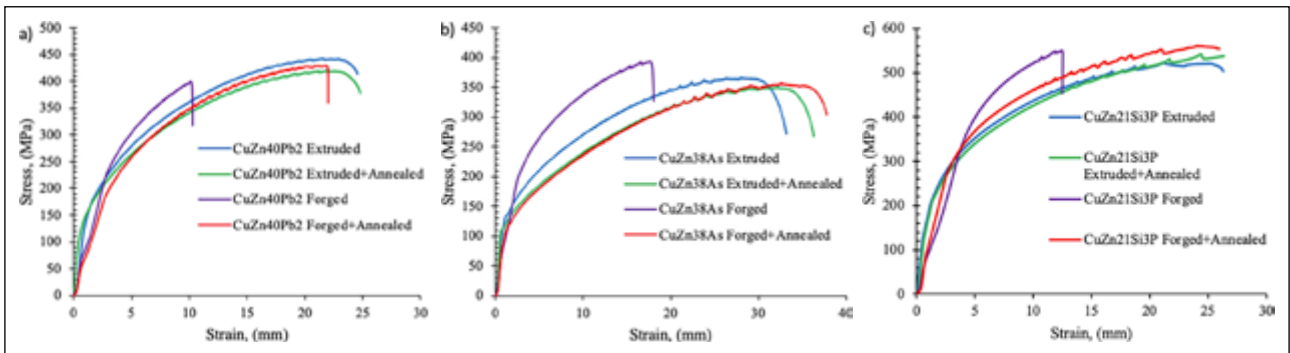


Figure 4. Tensile test plots; (a) CuZn40Pb2, (b) CuZn38As, (c) CuZn21Si3P.

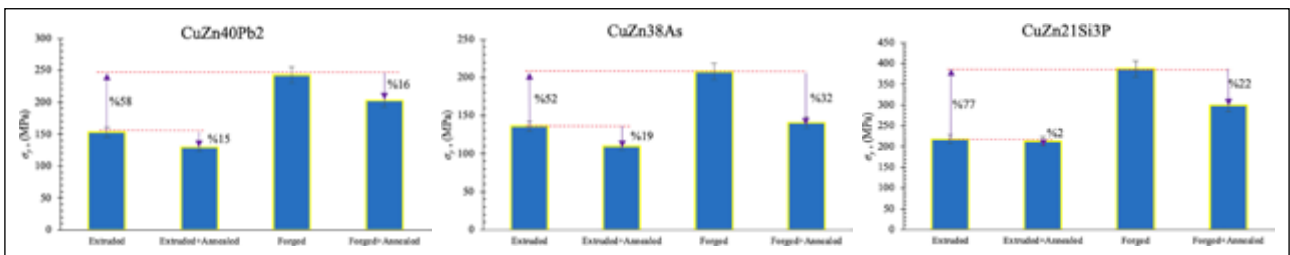


Figure 5. The yeild stress for the test materials.

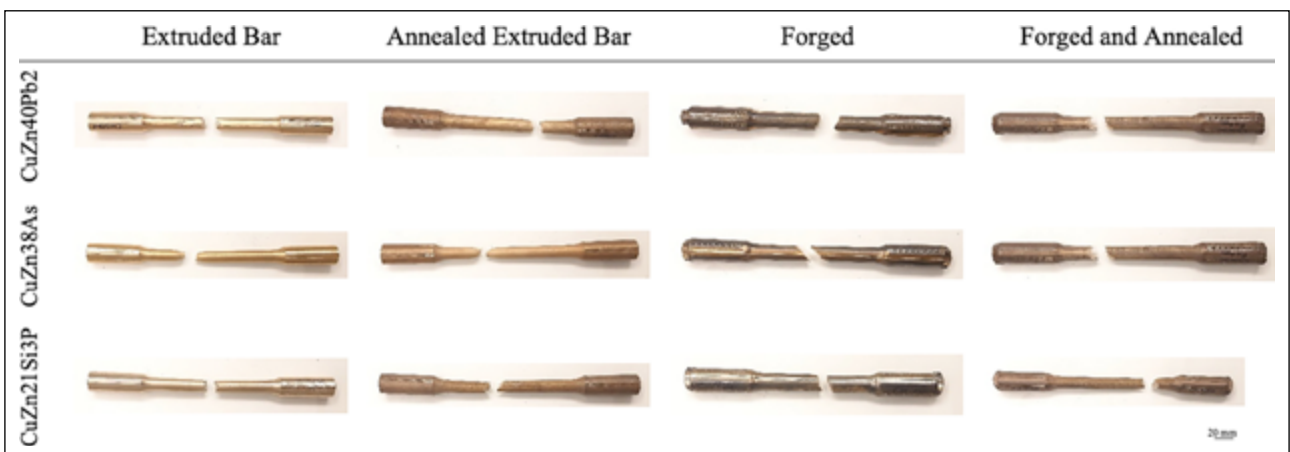


Figure 6. Ruptured images of the specimens after tensile test.

Table 5. The hardness results of the studied brass alloys

Brass type	Microhardness, (HV)
CuZn40Pb2	
Extruded	95.6
Extruded & annealed	92.3
Forged	107.9
Forged & annealed	98.5
CuZn38As	
Extruded	92.1
Extruded & annealed	88.8
Forged	102.3
Forged & annealed	96.7
CuZn21Si3P	
Extruded	118.2
Extruded & annealed	107.4
Forged	138.9
Forged & annealed	125.6

Table 6. The toughness results of the studied brass alloys

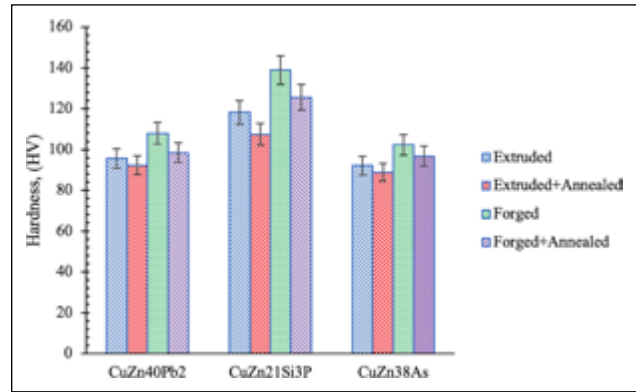
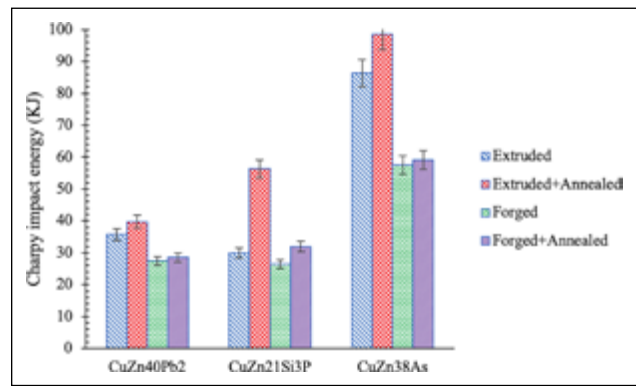
	Extruded bar	Extruded+ forged	Forged	Forged+ annealed
CuZn40Pb2	35.71	39.76	27.41	28.51
CuZn21Si3P	29.97	56.35	26.51	32
CuZn38As	86.26	98.55	57.6	59.12

Table 7. The first mode fracture toughness results of the studied brass alloys

	Extruded bar	Annealed extruded bar	Forged	Forged & annealed
CuZn40Pb2	429.54	364.97	682.20	569.91
CuZn21Si3P	612.02	597.98	1086.47	839.42
CuZn38As	381.81	308.82	583.94	339.70

The harder the material, the less tough and more plastic deformation is achieved. Prior to the writing of this paper, there were no published investigations on CuZn21Si3P that included impact fracture and annealing. Yet, the overall results of the microstructural investigations showed that annealing causes the formation of smaller grain sizes and boundaries.

The impact fractures' fractographic pictures are shown in Figure 8. Forged CuZn21Si3P has the lowest measured fracture energy of 26.51 KJ. However, for annealed extruded bar, the maximum value was measured at 98.55 KJ. As can be observed in Figure 9, the Charpy impact toughness effect produces an expressive distortion in the shape of the material CuZn38As that shows a greater strain before fracture. This form and the amount of absorbed energy are consistent with [15]. The shape deformation in CuZn21Si3P and CuZn40Pb2, however, is less than in CuZn38As due to

**Figure 7.** The measured hardness value for the brass alloys.**Figure 8.** The Charpy impact energy of the extruded, forged and annealed brass alloys.

the molecules' constraint from moving about and the lower energy needed to break atomic bonds, which results in less absorbed energy. In addition, it was discovered that annealing had increased the amount of energy absorbed for the reasons outlined in the section on the tensile test. Forging all of the test specimens, however, has lowered this rate.

Linear elastic materials' crack tips can experience mode I, II, III, or mixed occurrences depending on the stress type. These stresses can be expressed as a function of the fracture mode's stress intensity factor and polar or cartesian coordinate system. The process may be reduced into plane strain of mode I fracture, as illustrated in Figure 10, based on the impact Charpy test. Therefore, the first mode intensity factor and stresses can be expressed from Eq. 2 and 3.

Where K_{IC} , Y , σ and α are the first mode fracture toughness, geometric constant, yield stress and crack/notch length, respectively [25–27].

$$K_{IC} = Y\sigma\sqrt{\pi a} \quad (2)$$

$$\sigma_{xx} = \frac{K_{IC}}{\sqrt{2\pi r}} \cos\left(\frac{\theta}{2}\right) \left[1 - \sin\left(\frac{\theta}{2}\right) \sin\left(\frac{3\theta}{2}\right)\right] \quad (3)$$

$$\sigma_{yy} = \frac{K_{IC}}{\sqrt{2\pi r}} \cos\left(\frac{\theta}{2}\right) \left[1 + \sin\left(\frac{\theta}{2}\right) \sin\left(\frac{3\theta}{2}\right)\right] \quad (4)$$

$$\sigma_{yy} = \begin{cases} 0 & \text{plane stress} \\ v(\sigma_{xx} + \sigma_{yy}) & \text{plane strain} \end{cases} \quad (5)$$

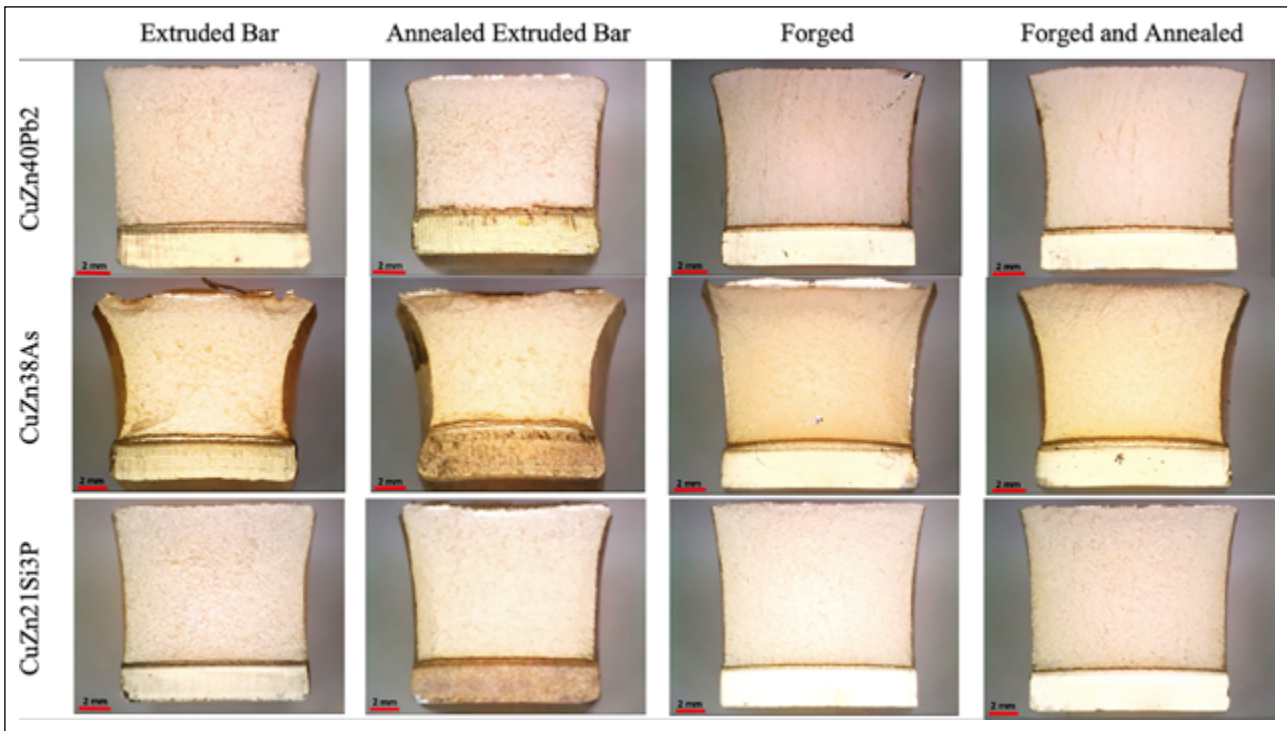


Figure 9. Fractographic images of the impact fractures.

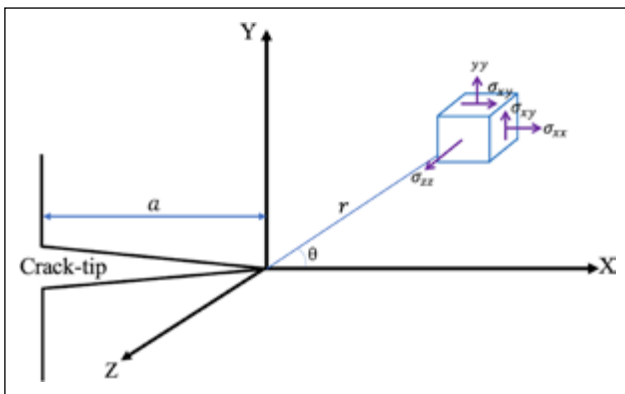


Figure 10. Schematic view of the first mode intensity factor and stresses.

$$\tau_{xy} = \frac{K_{IC}}{\sqrt{2\pi r}} \cos\left(\frac{\theta}{2}\right) \sin\left(\frac{\theta}{2}\right) \cos\left(\frac{3\theta}{2}\right) \quad (6)$$

$$\tau_{yz} = \tau_{xz} = 0 \quad (7)$$

The first mode fracture toughness values for the aforementioned brass alloys under various operational conditions are shown in Table 7 and Figure 11. The lowest first mode fracture toughness was calculated for annealed extruded bar CuZn38As as 308.82 MPa.m^{1/2}. However, the highest one was observed in forged CuZn21Si3P specimen as 1086.47 MPa.m^{1/2}. Based on the results, it can be said that forging is effective at improving the mechanical characteristics of the test materials since the structure is more refined. Additionally, because the specimens develop ductility during annealing, an improvement is also achieved.

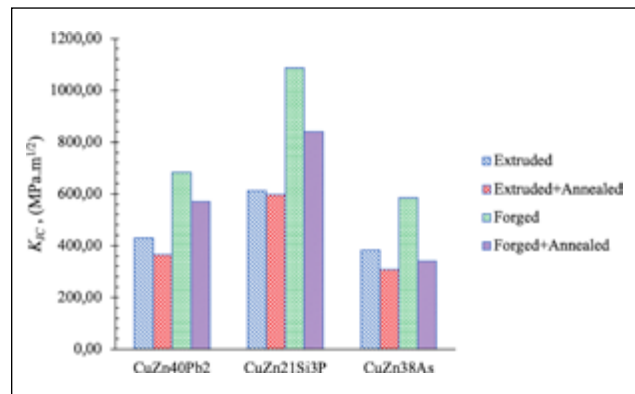


Figure 11. The calculated first mode fracture toughness values for the brass alloys.

CONCLUSION

In this study, the mechanical and metallurgical characteristics of an environmentally friendly CuZn38AS, and CuZn21Si3P brass alloys was compared with CuZn40Pb2. For this purpose, experiments on extruded, extruded+annealed, forged, and forged+annealed specimens were carried out. The investigation results for the influences of the process type on the microstructural, hardness, tensile, and impact properties is illustrated in the following conclusion:

Post-processing heat treatment on the studied dual α - β phase brass alloys has led to reduction in the β phase percentage. For the case of CuZn21Si3P, a decrease in the $\kappa\% + \gamma\%$ has been inspected. Furthermore, this post-processing caused a reduction of 15%, 19%, and 2% in the yield stress of the extruded bar for CuZn40Pb2, CuZn38As, and CuZn21Si3P, respectively, whereas these percentages were

16%, 41%, and 22% for the same forged materials. However, forging raised the yield stress by 58%, 52%, and 77% for CuZn40Pb2, CuZn38As, and CuZn21Si3P, respectively. An increase has been obtained in β by forging in all types of CuZn40Pb2 and CuZn38As. However, a reverse relation is accomplished by annealing on the mentioned alloys. For CuZn21Si3P, α has increased with annealing whereas it has been decreased by forging.

The hardness of the specimens was reduced by annealing. In the meantime, an increase in the hardness value is obtained as a result of the movement of the dislocations and grain refinements in the alloy structures extracted by forging process.

Annealing enhanced the toughness value for CuZn40Pb2, CuZn21Si3P, and CuZn38As by 11.34%, 88.02%, and 14.24%, respectively. In the case of forged specimens, annealing resulted in increases in the fracture energy values of CuZn40Pb2, CuZn21Si3P, and CuZn38As of 4.03%, 20.70%, and 2.64%, respectively.

Acknowledgements

The authors thank TUBITAK (The Scientific and Technological Research Council of Türkiye) for partially supporting this work under project number 118C069.

Data Availability Statement

The authors confirm that the data that supports the findings of this study are available within the article. Raw data that support the finding of this study are available from the corresponding author, upon reasonable request.

Author's Contributions

Nima Zoghypour: Design of experiments, Performing the experiments, preparing the article.

Yusuf Kaynak: Supervisor.

Conflict of Interest

The authors declared no potential conflicts of interest with respect to the research, authorship, and/or publication of this article.

Ethics

There are no ethical issues with the publication of this manuscript.

REFERENCES

- [1] Imai, H., Kosaka, Y., Kojima, A., Li, S., Kondoh, K., Umeda, J., & Atsumi, H. (2010). Characteristics and machinability of lead-free P/M Cu60–Zn40 brass alloys dispersed with graphite. *Powder Technology*, 198, 417–421. [CrossRef]
- [2] Pantazopoulos G., & Vazdirvanidis A. (2008). Characterization of the microstructural aspects of machinable α - β phase brass. *Microscopy and Analysis*, 13–16.
- [3] Pantazopoulos, G., & Vazdirvanidis, A. (2008). Failure analysis of a fractured leaded brass (CuZn-39Pb3) extruded hexagonal rod. *Journal of Failure Analysis and Prevention*, 8, 218–222. [CrossRef]
- [4] Toulfatzis, A. I., Besseris, G. J., Pantazopoulos, G. A., & Stergiou, C. (2011). Characterization and comparative machinability investigation of extruded and drawn copper alloys using non-parametric multi response optimization and orthogonal arrays. *International Journal of Advanced Manufacturing Technology*, 57, 811–826. [CrossRef]
- [5] D'Mellow, B., Thomas, D. J., Joyce, M. J., Kolkowski, P., Roberts, N. J., & Monk, S. D. (2007). The replacement of cadmium as a thermal neutron filter. *Nuclear Instruments and Methods in Physics Research Section A: Accelerators, Spectrometers, Detectors and Associated Equipment*, 577, 690–695. [CrossRef]
- [6] Switch Electronics. (2017). RoHS and WEEE compliant flame retardants developed for electrical connectors. [https://www.switchelectronics.co.uk/rohs-weee-and-reach ReinfPlastics](https://www.switchelectronics.co.uk/rohs-weee-and-reach-ReinfPlastics), 51(8), 12. [CrossRef]
- [7] Mans, C., Hanning, S., Simons, C., Wegner, A., Janßen, A., & Kreyenschmidt, M. (2007). Development of suitable plastic standards for X-ray fluorescence analysis. *Spectrochimica Acta Part B: Atomic Spectroscopy*, 62(2), 116–122. [CrossRef]
- [8] Brass for European Potable Water Applications. (2020). <https://www.copper.org/applications/rod-bar/pdf/A7038-brass-for-european-potable-water-applications.pdf>
- [9] Trends in Sales of ECO BRASS. (2020). https://rohs.exemptions.oeko.info/fileadmin/user_upload/RoHS_Pack_9/Exemption_6_c_/Exemption_6c__2015-10-mitsubishi-shindoh-rohs.pdf
- [10] Chen, X., Hu, A., Li, M., & Mao, D. (2008). Study on the properties of Sn–9Zn–xCr lead-free solder. *Journal of Alloys and Compounds*, 460, 478–484. [CrossRef]
- [11] Kuyucak, S., & Sahoo, M. (1996). A review of the machinability of copper-base alloys. *Canadian Metallurgical Quarterly*, 35(1), 1–15. [CrossRef]
- [12] Holler, K., Reetz, B., Müller, K. B., & Pyzalla, A., & Reimers, W. (2003). Microstructure and properties of hot extruded brass CuZn40Pb2. *Materials Science Forum*, 426–432, 3667–3672. [CrossRef]
- [13] Stålnacke, E., Claesson, E., Obitz, C., Lilja, M., Odqvist, J., Hagström, J., & Rod, O. (2018). Corrosion–microstructure interrelations in new low-lead and lead-free brass alloys. *Materials Science and Technology*, 36, 917–924. [CrossRef]
- [14] Toulfatzis, A. I., Pantazopoulos, G. A., David C. N., Sagris D. S., Paipetis A. S. (2018). Final heat treatment as a possible solution for the improvement of machinability of Pb-free brass alloys. *Metals*, 8, Article 575. [CrossRef]
- [15] Toulfatzis A. I., Pantazopoulos G. A., & Paipetis A. S. (2014). Fracture behavior and characterization of lead-free brass alloys for machining applications. *Journal of Materials Engineering and Performance*, 23, 3193–3206. [CrossRef]
- [16] Pantazopoulos G. A., & Toulfatzis A. I. (2012). Fracture modes and mechanical characteristics of machinable brass rods. *Metallography, Microstructure, and Analysis*, 1, 106–114. [CrossRef]

- [17] Chunlei, G., Nan, Z., Yuehua, K., Shuncheng, W., Kaihong, Z. (2019). Failure analysis of lead-free brass valve bodies. *Engineering Failure Analysis*, 100, 536–543. [CrossRef]
- [18] Amaral, L., Quinta R., Silva T. E., Soares, R. M. B., Castellanos, S. D., & de Jesus, A. M. P. (2018). Effect of lead on the machinability of brass alloys using polycrystalline diamond cutting tools. *The Journal of Strain Analysis for Engineering*, 53, Article 030932471879638. [CrossRef]
- [19] Sarbak. (2020). *Alloy*. <https://www.sarbak.com.tr/en/documents/alloys>
- [20] Schultheiss, F., Johansson, D., Bushlya, V., Zhou, J., Nilsson, K., & Ståhl, J. E. (2015). Comparative study on the machinability of lead-free brass. *Journal of Cleaner Production*, 149, 366–377. [CrossRef]
- [21] Zoghipour, N., Tascioglu, E., Atay, G., & Kaynak, Y. (2020). Machining-induced surface integrity of holes drilled in lead-free brass alloy. *Procedia CIRP*, 87, 148–152. [CrossRef]
- [22] Davis, J. R., Davidson, G. M., Lampman, S. R. & Zorc, T. B. (1997). *Heat Treating*, ASM International, Materials Park, Ohio, 841–879.
- [23] Doostmohammadi, H., & Moridshahi, H. (2015). Effects of Si on the microstructure, ordering transformation and properties of the Cu60Zn40 alloy. *Journal of Alloys and Compounds*, 640, 401–407. [CrossRef]
- [24] Callister, W.D. (2001). *Fundamentals of Materials Science and Engineering*, (2nd ed). Wiley & Sons, 252.
- [25] C. H. Wang, Introduction to fracture mechanics. Melbourne, Vic.: DSTO Aeronautical and Maritime Research Laboratory, 1996.
- [26] E. Şar, Tensile opening mode fracture toughness measurements and size effect investigations with Brazilian disc type rock specimens, Middle East Technical University, 2020.
- [27] Toulfatzis, A., Pantazopoulos, G., & Paipetis, A. (2016). Microstructure and properties of lead-free brasses using post-processing heat treatment cycles. *Materials Science and Technology*, 32, 1771–1781. [CrossRef]